Physics of the 9-Month Variability in the Gulf Stream Region: Combining Data and Dynamical Systems Analyses

MAURICE J. SCHMEITS AND HENK A. DIJKSTRA

Institute for Marine and Atmospheric Research Utrecht, Department of Physics and Astronomy, Utrecht University, Utrecht, Netherlands

(Manuscript received 11 February 1999, in final form 20 September 1999)

ABSTRACT

Using nonseasonal altimeter data and SST observations of the North Atlantic, and more specifically the Gulf Stream region, dominant patterns of variability are determined using multivariate time series analyses. A statistically significant propagating mode of variability with a timescale close to 9 months is found, the latter timescale corresponding to dominant variability found in earlier studies. In addition, output from a high resolution simulation of the Parallel Ocean Climate Model (POCM) is analyzed, which also displays variability on a timescale of 9 months, although not statistically significant at the 95% confidence level. The vertical structure of this 9-month mode turns out to be approximately equivalent barotropic. Following the idea that this mode is due to internal ocean dynamics, steady flow patterns and their instabilities are determined within a barotropic ocean model of the North Atlantic using techniques of numerical bifurcation theory. Within this model, there appear to be two different mean flow paths of the Gulf Stream, both of which become unstable to oscillatory modes. For reasonable values of the parameters, an oscillatory instability having a timescale of 9 months is found. The connection between results from the bifurcation analysis, from the analysis of the observations, and from the analysis of the POCM output is explored in more detail and leads to the conjecture that the 9-month variability is related to a barotropic instability of the wind-driven gyres.

1. Introduction

The Gulf Stream is one of the most intense western boundary currents in the global ocean. From the enormous amount of data now available and thoroughly analyzed (Richardson 1985; Auer 1987; Hall and Fofonoff 1993; Qiu 1994), the time mean path is quite well known. Starting from the south, the current flows almost parallel to the coastline and at Cape Hatteras, it leaves the North American continent and flows northeastward past the Grand Banks. After separation, there is increased meandering, but the stream keeps a mean latitudinal position of about 40°N up to 50°W. Near Cape Hatteras, the volume transport is estimated to be about 50–65 Sv (Sv $\equiv 10^6$ m^3 s^{-1}), which increases to a total of about 145 Sv at 60°W (Johns et al. 1995).

Since the current transports a significant amount of heat northward, it is important to understand its temporal variability on different timescales. In early days, this variability has been studied using in situ data (Hansen 1970; Fuglister 1972) but more recently these data have been complemented with satellite-derived observations. At the moment, there is a sufficiently long time series to study variability on timescales up to a year in quite detail. In Table 1, details of the spatial and temporal resolution of the data and the methods of analysis are given for several of these studies. Maul et al. (1978) used infrared measurements from the Geostationary Operational Environmental Satellite (GOES) mission over a two-year (1976–78) period and found a dominant timescale of 45 days in the meandering of the Gulf Stream near New England. Using a combination of infrared data and observations of sea-level height anomalies derived from the GEOSAT altimeter over the period November 1986–December 1988, Vazquez et al. (1990) concluded that the annual signal in Gulf Stream variability is dominated by the meandering of the current. The latter study was extended in Vazquez (1993), using complex empirical orthogonal function (CEOF) analysis on the same dataset. It appeared that four CEOFs could account for 60% of the variability and each of these represented different propagating signals, which were shown to be related to Rossby wave propagation, eddy–stream interactions, and bottom topography.

Data from cycles 3–54 from the TOPEX/Poseidon mission were analyzed by Wang and Koblinsky (1995), and three dominant modes of variability were identified

Corresponding author address: Henk A. Dijkstra, Institute for Marine and Atmospheric Research Utrecht, Department of Physics and Astronomy, Utrecht University, Princetonplein 5, 3584 CC Utrecht, Netherlands.
E-mail: dijkstra@phys.uu.nl

TABLE 1. Overview of studies of the Gulf Stream region using satellite data.

Reference	Data, Period	Domain	Resolution
Auer (1987)	infrared, 1980–85	91°–44°W	Weekly, 0.5°
Maul et al. (1978)	infrared, 1976–78	86°–70°W	Daily, pointwise
Vazquez et al. (1990)	GEOSAT, 1986–88	80°–50°W	Weekly, 0.5°
Vazquez (1993)	GEOSAT, 1986–88	75°–60°W	10 days, 0.25°
Wang and Koblinsky (1995)	TP, cycles 3–54	80°–30°W	10 days, 1°
Lee and Cornillon (1995)	AVHRR, 1982–89	75°–60°W	2 days, 20 km
Kelly et al. (1996)	GEOSAT + ECMWF	75°–45°W	1 day, 1°
Wang and Koblinsky (1996)	TP, 74 cycles + GEOSAT	80°–30°W	10 days, 1°
This study	TP, 154 cycles + SST	97°–32°W	10 days/1 month, 1°

through empirical orthogonal function (EOF) analysis. The first EOF was associated with the seasonal cycle but the second EOF showed low-frequency wave activity (of about annual period), and by computing eddy kinetic energies and the Reynolds stresses they concluded that bottom topography plays an essential role in the latter component of variability. The third EOF had a period of 8 months and external forcing through bottom topography was suggested as the generation mechanism.

Using AVHRR-derived infrared images for the period April 1982 through December 1989, Lee and Cornillon (1995) found two dynamically distinct modes of variability of the path of the Gulf Stream. The first mode of variability is associated with large-scale lateral shifts of the mean path having a near-annual period. These shifts are presumably caused by atmospheric forcing, partly through the changes in downward heat flux (Wang and Koblinsky 1996) and partly through the changes in wind forcing over the area (Kelly et al. 1999). The second mode of variability is associated with changes in meandering intensity having a 9-month dominant periodicity. The cause of the 9-month periodicity in meandering intensity is not explained but Lee and Cornillon (1995) suggest that it is related to internal oceanic dynamics.

Near-annual variability is also found in recent studies of the Kuroshio extension. Wang et al. (1998) find that the first CEOF has an average period of 9 months and its spatial pattern indicates a rotation of a double-cell pattern around the axis of the mean flow. Using both ECMWF atmospheric fields and Geosat data, Kelly et al. (1996) also found this type of variability in both the Gulf Stream and the Kuroshio. For both western boundary currents, it was attributed to structural changes in the recirculation gyres, associated with a path change. The variations in the Gulf Stream have largest amplitudes east of 62°W and were not strongly related to heat flux variations over the area.

From all the work above, it is clear that variations in the path of the Gulf Stream exist on a timescale that is slightly smaller than annual and that is unlikely to be caused directly by variations in atmospheric forcing. Internal ocean dynamics, that is, intrinsic variability due to nonlinear interactions in the current itself, are a likely origin, but the question is whether a clear candidate of such mode of variability can be found.

Recently, the stability and variability of the double gyre wind-driven ocean circulation has been investigated systematically within an hierarchy of models (Jiang et al. 1995; Cessi and Ierley 1995; Speich et al. 1995; Dijkstra and Katsman 1997; Katsman et al. 1998; Dijkstra and Molemaker 1999). Bifurcations mark the transitions between different regimes of behavior and a bifurcation diagram describes the behavior of the dynamical system in phase space. Hopf bifurcations are important in the study of the origin of a particular type of variability because they mark the transition to temporal behavior. Using 1.5-layer quasigeostrophic (QG) models (Cessi and Ierley 1995; Dijkstra and Katsman 1997) and 1.5-layer shallow water (SW) models (Jiang et al. 1995; Dijkstra and Molemaker 1999) in rectangular basins, it was found that the idealized double gyre flows become unstable to two types of barotropic modes: basin modes and gyre modes. The timescales of the former are a couple of months, whereas the latter instabilities have time scales in the order of years. In two-layer QG models (Dijkstra and Katsman 1997; Katsman et al. 1998), additional baroclinic instabilities appear having an intermonthly timescale.

By using a hierarchy of β-plane models, starting from a 1.5-layer QG model in a rectangular basin with sinusoidal wind stress forcing toward a 1.5-layer shallow water model in a basin with realistic geometry and wind-stress forcing, Dijkstra and Molemaker (1999) found that the basic structure of the steady states and most unstable modes remains qualitatively intact. Multiple equilibria found in the QG model ''deformed'' into multiple flow paths of the Gulf Stream. Furthermore, the modes of variability remained closely related, seemed to depend only on the local properties of the gyres near the western boundary, and were not much influenced by the geometry of the basin.

Since some of these dynamical modes have near-annual timescales, we investigate in this paper the hypothesis that the origin of the 9-month variability found in the Gulf Stream region is a barotropic instability of the western boundary current/midlatitude jet system of the North Atlantic. The approach is along three paths: First, multivariate time series analysis techniques will

be used to extract statistically significant modes of variability in sea surface temperature (SST) and sea surface height (SSH) observations. Second, output from the Parallel Ocean Climate Model (POCM) (Semtner and Chervin 1992; Stammer et al. 1996) is analyzed with the same statistical techniques giving information on the vertical structure of the variability. Finally, the instabilities of the barotropic North Atlantic wind-driven circulation will be studied within a full basin-scale barotropic shallow-water model with realistic geometry and forcing. The observations and POCM output used in this study are presented in section 2 together with a short recapitulation of the analysis technique. The results of the data analysis and of the shallow-water model's bifurcation analysis are given in sections 3 and 4, respectively, with a discussion in section 5.

2. Data and analysis technique

a. Observations and POCM output

The datasets used in this study are monthly SST fields from Reynolds and Smith (1994), relative sea surface height observations from the NASA TOPEX/Poseidon Altimeter Pathfinder (T/P) Dataset and output from run 4C of POCM. The SST data are derived from a blend of remotely sensed and in situ data and then subjected to an optimum interpolation (OI) analysis (Reynolds and Smith 1994). The monthly SST fields are provided on a regular 1° latitude/longitude grid. For the separate analysis of SST we use data in the Gulf Stream region (24°–48°N, 97°–32°W) from 1982–1996.

The T/P dataset consists of time, positions, and relative sea surface height observations to which all types of corrections have been applied over cycles 1–154. The data processing used to construct the dataset has been described at http://neptune.gsfc.nasa.gov/~krachlin/opf/algorithms.html. The satellite orbit results in repeated ground tracks every 10 days. A mean relative sea surface height was computed at each grid point for all 154 cycles. Residual SSH anomalies are then computed by subtracting the mean relative sea level from each observation. Outliers (SSH anomalies > 1.5 m) are excluded from the dataset.

The SSH anomalies along ground tracks are interpolated in space to a regular 1° latitude/longitude grid and in time to a resolution of 10 days for the separate analysis of SSH and to 1 month for the combined analysis of SSH and SST. A Gaussian interpolation is used with a decorrelation scale of 2° and a cutoff radius of 6° in space and a decorrelation scale of 10 days and a cut off of 30 days in time. The cutoff radius of 6° corresponds to the Nyquist wavenumber for the 3-degree T/P track spacing. Although the Gaussian interpolation is not equivalent to a low-pass filter with a cut off of 6°, all wavelengths up to the decorrelation scale of 2° have been filtered out and about 65% of the amplitudes of the wavelength of 6° (Vossepoel 1995). The choice of the spatial decorrelation scale is a compromise between avoiding aliasing on the one hand and retaining the interpolated signal well above the measurement error on the other hand. For the separate analysis of SSH and the combined analysis of SST and SSH we use data in the same region as above from November 1992 to November 1996.

The POCM output is from run 4C having an average horizontal resolution of 0.25° and 20 nonequidistant levels in the vertical direction. The basic model formulation has been described by Semtner and Chervin (1992). The global simulation was performed over the period 1979–97 and the ocean was forced by either ECMWF reanalysis (1979–93) or ECMWF operational (1994–97) fields of heat fluxes, freshwater fluxes, and wind stress. These fields are updated every 3 days and interpolated to the time step. The annual river outflow was also included in the freshwater flux. For more details about this simulation the reader is referred to http://vislab-www.nps.navy.mil/~rtt. We have used monthly mean SST, SSH, and temperature fields at two depth levels, namely 310 m (T310) and 610 m (T610), in the Gulf Stream region (23°–48°N, 90°–30°W) from 1979 to 1997. SSH is a prognostic variable in POCM because of the incorporation of a free surface formulation.

The seasonal cycle has been eliminated from the SST dataset by computing anomalies about the 1982–96 monthly climatology, from the SSH dataset by calculating anomalies about the 1992–96 10-daily/monthly climatology, and from the POCM output by computing anomalies about the 1979–97 monthly climatology. In this way, effects of the seasonal atmospheric forcing have been removed from the datasets. No further filtering of the datasets has been undertaken, apart from prefiltering with principal component analysis (PCA) (Preisendorfer 1988) in order to reduce the number of spatial degrees of freedom in the datasets. Finally, the statistical mean at each point has been removed prior to the analysis.

b. Data analysis method

The time series fields from the datasets are analyzed with the aid of a pattern analysis technique designed to empirically infer the characteristics of the space–time variations of a complex system.

The technique that we used is multichannel singular spectrum analysis (M-SSA) (Plaut and Vautard 1994), which produces propagating patterns that are optimal in representing variance. The aim of using M-SSA is to identify coherent space–time patterns, given a regularly sampled archive of maps. M-SSA is mathematically equivalent to extended EOF analysis (EEOF) (Weare and Nasstrom 1982), but in M-SSA focus is on the temporal structure of the variability, whereas in EEOF the spatial variability is emphasized.

The essentials of the technique are summarized here to introduce terminology used below. Let a dataset **X**

consist of a multichannel time series $\mathbf{X}_{l,i}$, $i = 1, \cdots, N$; $l = 1, \cdots, L$, where i represents time and l the channel number. Index l may represent a point number on a specific grid or a principal component (PC) if the data are pre-filtered with PCA. We assume that $\mathbf{X}$ has zero mean and is stationary. By making M lagged copies of $\mathbf{X}$, the state vector at time i is given by

$$(\mathbf{X}_{1,i+1}, \mathbf{X}_{1,i+2}, \ldots, \mathbf{X}_{1,i+M}, \mathbf{X}_{2,i+1}, \ldots, \mathbf{X}_{2,i+M}, \ldots, \mathbf{X}_{L,i+1}, \ldots, \mathbf{X}_{L,i+M}), \quad (1)$$

where M is the window length. The cross-covariance matrix $\mathbf{T}$ for a chosen window length M has a general block-Toeplitz form in which each block $\mathbf{T}_{ll'}$ is the lag covariance matrix (with maximum lag M) between channel l and channel l'. The $L \times M$ real eigenvalues λ_k of the symmetric matrix $\mathbf{T}$ are sorted in decreasing order where an eigenvector (referred to as a ST–EOF) $\mathbf{E}^k$ is associated with the kth eigenvalue λ_k. The $\mathbf{E}^k$ are M-long time sequences of vectors, describing space–time patterns of decreasing importance as their order k increases. A space–time principal component (referred to as a ST-PC) a^k can be computed by projecting $\mathbf{X}$ onto $\mathbf{E}^k$; λ_k is the variance in a^k. In this way, the M-SSA expansion of the original data series is given by

$$\mathbf{X}_{l,i+j} = \sum_{k=1}^{L\times M} a_i^k \mathbf{E}_{lj}^k, \qquad j = 1, \cdots, M. \quad (2)$$

Principal component analysis (Preisendorfer 1988) and single-channel singular spectrum analysis (SSA) (Vautard and Ghil 1989; Vautard et al. 1992) are particular cases of M-SSA: PCA can be derived from M-SSA with $M = 1$, and SSA with $L = 1$.

When two consecutive eigenvalues are nearly equal and the two corresponding $\mathbf{E}^k$ as well as the associated a^k are in quadrature, then the data possess an oscillation whose period is given by that of a^k and whose spatial pattern is that of $\mathbf{E}^k$ (Plaut and Vautard 1994). The sum in the right-hand side of (2), restricted to one or several terms, describes the part of the signal behaving as the corresponding $\mathbf{E}^k$. The components constructed in this way are called reconstructed components (RCs). In this way, the part of the signal involved with an oscillation can be isolated. The original signal is exactly the sum of all the RCs.

As Allen and Robertson (1996) have pointed out, the presence of an eigenvalue pair is not sufficient grounds to conclude that the data exhibits an oscillation. Moreover, low-frequency eigenvalue pairs, which are entirely due to red noise, will appear high in the eigenvalue rank-order. A Monte Carlo red-noise significance test for M-SSA was therefore constructed (Allen and Robertson 1996). This is an objective hypothesis test for the presence of oscillations at low signal-to-noise ratios in multivariate data. Rejection of the red-noise null hypothesis using the test should be considered a necessary condition for M-SSA to have detected an oscillation, although in certain situations nonoscillatory processes might also lead to rejection.

The test is built up as follows. Surrogate data segments are constructed by superposing L uncorrelated AR(1) processes having the same variance and lag-1 autocorrelation as the PCs (from standard PCA) of the dataset. Data and surrogate data segments are then projected onto a ST-PC basis of rank $N - M + 1$. This basis is either derived from the data cross-covariance (Toeplitz) matrix (referred to as the data-adaptive basis) or from the AR(1) process cross-covariance matrix (referred to as the null-hypothesis basis). The matrix of projections $\mathbf{\Lambda}$ is

$$\mathbf{\Lambda} \equiv \mathbf{P}^{\mathrm{T}}\mathbf{Y}\mathbf{Y}^{\mathrm{T}}\mathbf{P}, \quad (3)$$

where $\mathbf{Y}$ is the augmented data matrix of either red-noise surrogate data, or the sample time series, and $\mathbf{P}$ is the ST–PC basis. The method is described in detail by Allen and Robertson (1996).

3. Results of the data analysis

a. Spatiotemporal variability of SST observations

To reduce the number of spatial dimensions, we initially perform a conventional PCA of the normalized nonseasonal SST data and retain 24 PCs, which account for 90% of the variance. These PCs provide the L input channels for the M-SSA algorithm. We have 15 years of data, so $N = 180$, and use a standard window length M of 60 months.

The Monte Carlo significance test for M-SSA (Allen and Robertson 1996) is applied first in order to investigate which oscillating patterns contain more variance than would be expected if the data were generated by red noise. Both data and surrogates are projected onto the ST–PCs of the null-hypothesis basis (Allen and Robertson 1996) and the result is shown in Fig. 1a. Three data eigenvalues, with associated frequencies 0.11, 0.15, and 0.18 month^{-1}, are found to be significant. Now we have used the null-hypothesis basis to establish that there is some evidence of oscillations, we have to examine the data-adaptive basis for pairs of ST–PCs, which characterize those oscillations (Allen and Robertson 1996). In Fig. 1b both data and surrogates are projected onto the data ST–PCs. The test has picked out three pairs associated with the same frequencies as the ones that were indicated as significant in Fig. 1a. The most dominant pair of these three is ST–PC 7–8 (Fig. 1b), which explains 7% of the variance in the 24 leading PCs. This is not much, but the test has indicated that the first six ST–PCs (which together explain 26% of the variance in the 24 leading PCs) contain no more variance than would be expected if the data would consist of a set of independent AR(1) processes.

To check the robustness of these results with respect to different values of the window length M, Table 2 shows the timescales, indicated as significant by the

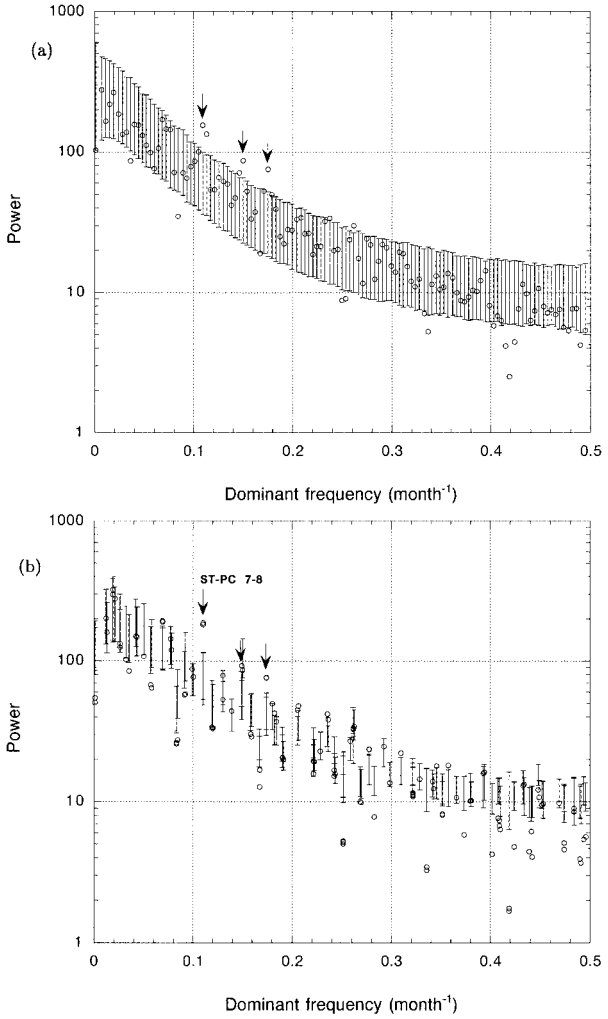

FIG. 1. Monte Carlo significance test of nonseasonal monthly SST data in the Gulf Stream region for the period 1982–1996, using $L = 24$ PCs from a conventional PCA as the input channels. Shown are projections of the SST data onto (a) the AR(1) null-hypothesis basis and (b) the data-adaptive basis, with a 60-month window ($M = 60$). Open circles show the data eigenvalues, plotted against the dominant frequency of the corresponding ST–PC. The vertical bars show the 95% confidence interval computed from 1000 realizations of a noise model consisting of L independent AR(1) processes with the same variance and lag-1 autocorrelation as the input data channels.

Monte Carlo test for M-SSA, for M between 40 and 80 months. It is clear from this table that the variability on timescales of 9 and 6 months is robust.

As can be seen in Fig. 2, ST–PC 7 and 8 are in quadrature, which suggests that the pair represents an oscillating statistical mode (Plaut and Vautard 1994) with a dominant period of 9 months. The same 9-month mode was also indicated as significant in the case where the domain of analysis was extended to the whole North Atlantic basin. In order to isolate the part of the signal involved with this oscillation RC 7–8 has been calculated and the reconstructed anomaly patterns of SST have been plotted in Fig. 3 for five phases during the oscillation. The starting time was chosen to be October 1985, when meandering intensity was at its maximum in the 1980s (Lee and Cornillon 1995) and each subsequent picture is 1 month later showing nearly half of the period of the oscillation. The maximum amplitude of the anomalies is 0.6 K.

TABLE 2. Output from the Monte Carlo significance test for M-SSA on the SST data for M between 40 and 80 months.

M (months)	Significant periods (months)
40	9, 6
60	9, 7, 6
80	9, 6, 4

In Fig. 3 two SST anomalies of opposite sign are rotating in a counterclockwise fashion in and just to the north of the mean axis of the Gulf Stream, whose latitudinal position increases from 39° to 44°N in the longitudinal band from 65° to 45°W (Auer 1987). These anomalies are pinched off from another oscillation (in the region 30°–42°N, 75°–65°W), where two SST anomalies of opposite sign are rotating in a clockwise fashion. This is the region where the Gulf Stream has just separated from the North American continent. A third pair of opposite anomalies is rotating in a counterclockwise fashion in the Gulf of Mexico.

b. Spatiotemporal variability of SSH observations

To investigate whether the 9-month periodicity found in the SST observations can also be found in another dataset, we have analyzed the SSH dataset. Due to the removal of the seasonal cycle, the signature of the steric response to the seasonal heating cycle has been removed, leaving the signature of barotropic and baroclinic changes in ocean circulation (Kelly et al. 1999). As in the case of SST, the normalized nonseasonal SSH anomalies were first submitted to a standard PCA analysis and only the leading 22 PCs retained, which account

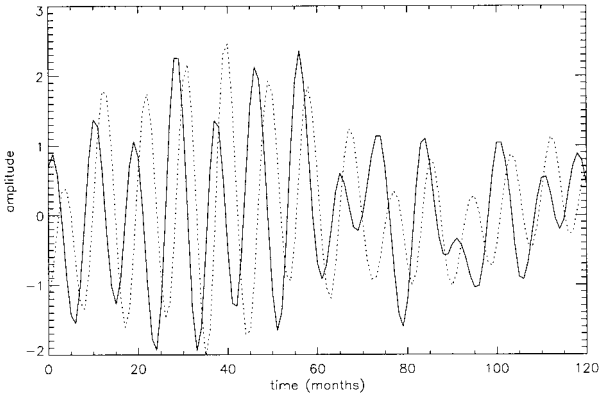

FIG. 2. Time series of M-SSA principal component (ST-PC) pair 7–8 of Gulf Stream SST; the amplitude scale is arbitrary. The 10-yr time span in the horizontal axis corresponds to $N - M + 1$, which is the length of the ST-PC time series.

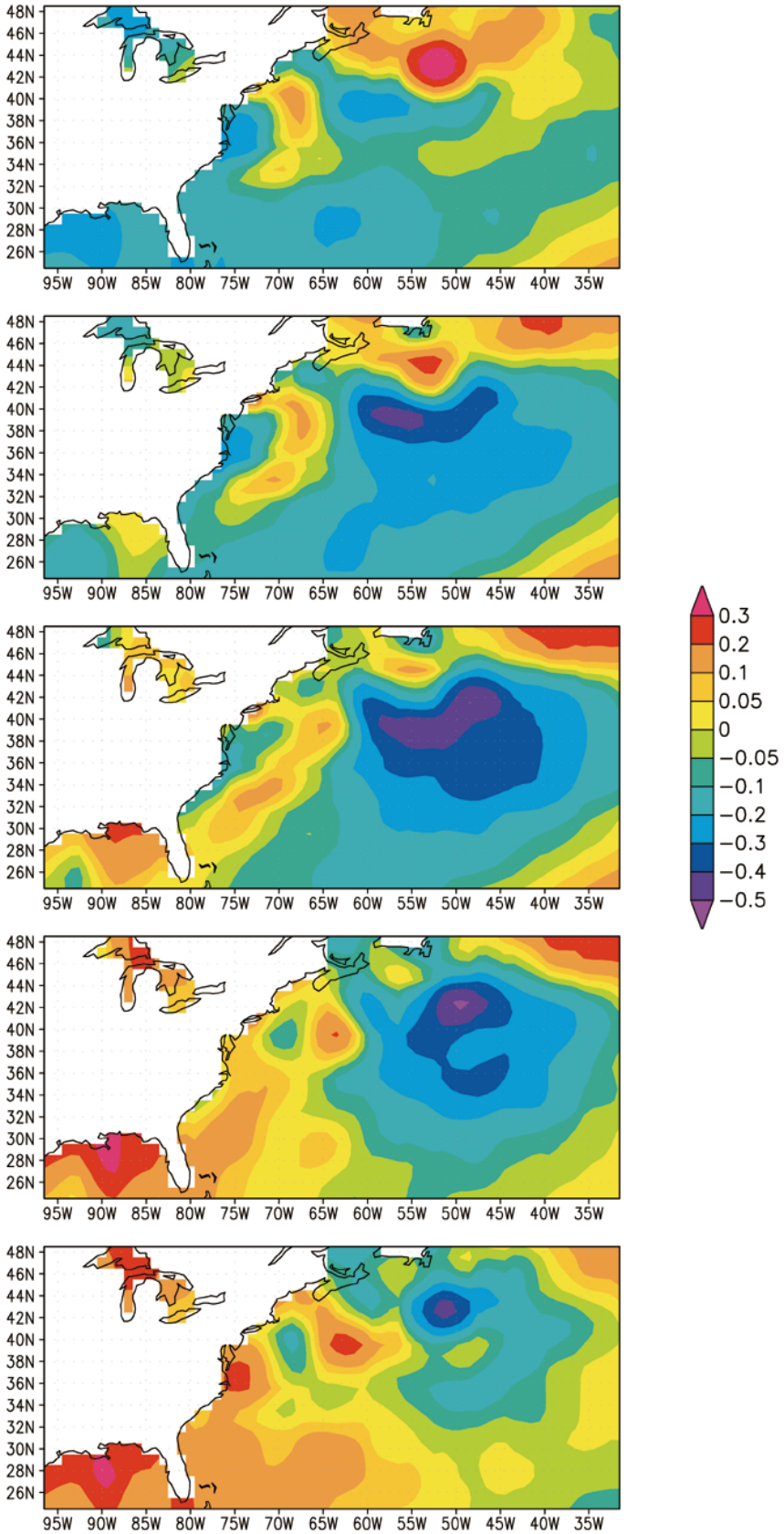
48N
46N
44N
42N
40N
38N
36N
34N
32N
30N
28N
26N
95W 90W 85W 80W 75W 70W 65W 60W 55W 50W 45W 40W 35W
0.3
0.2
0.1
0.05
0
−0.05
−0.1
−0.2
−0.3
−0.4
−0.5

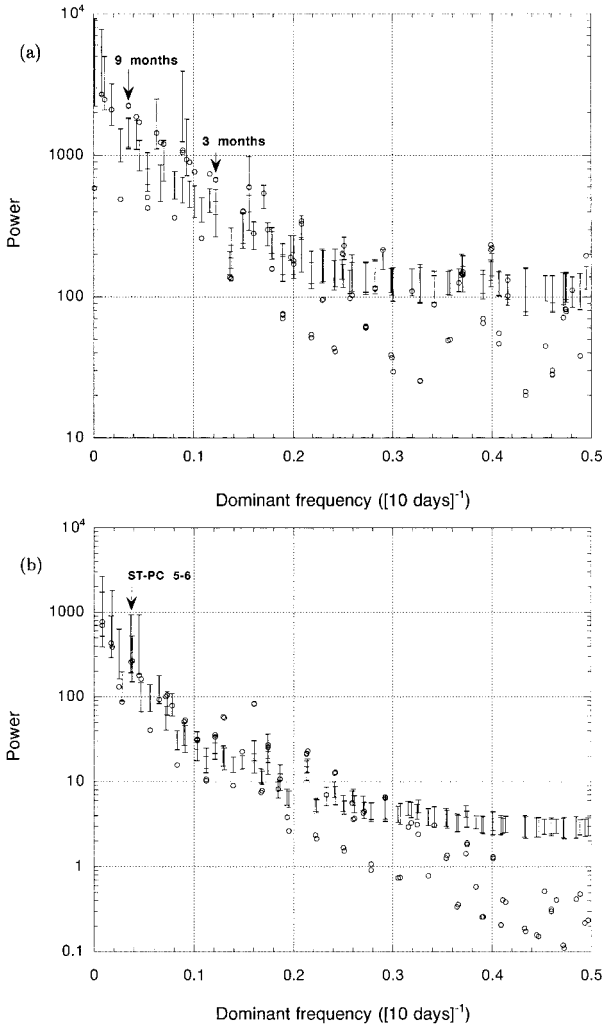

FIG. 4. Monte Carlo significance test of (a) uninterpolated and (b) interpolated nonseasonal TOPEX/Poseidon SSH data in the Gulf Stream region for the period Nov 1992–Nov 1996, using (a) $L = 41$ and (b) $L = 22$ PCs from a conventional PCA as the input channels. Shown are projections of the SSH data onto the data-adaptive basis, similar to that in Fig. 1b, with (a) $M = 50$ and (b) $M = 48$.

for 91% of the variance. These PCs provide the L input channels for the M-SSA algorithm. We have 4 years of data, so $N = 144$. We have used a window length of 480 days ($M = 48$).

Again, first the Monte Carlo significance test for M-SSA has been applied. Because the test result depends on the values of the interpolation parameters (i.e., the decorrelation scales of the Gaussian interpolation), the result is shown for both the uninterpolated and interpolated datasets in Figs. 4a and 4b, respectively. In Fig. 4a, anomalous power against the red-noise hypothesis is observed in two different ST–PC pairs, associated with periods of 9 and 3 months, respectively. In the interpolated dataset the dominant time scale of 9 months belongs to ST–PC pair 5–6 (Fig. 4b), which explains 11% of the variance in the 22 leading PCs. This pair is, however, not significant at the 95% confidence level as a result of the smoothing process, which reduces the signal's amplitude to a large extent. The maximum amplitude of the 9-month statistical mode in the uninterpolated dataset is 31 cm, whereas the maximum amplitude of this mode in the interpolated dataset is only 5 cm. It turns out that ST–PC 5 and 6 are in quadrature as are the corresponding ST-EOF 5 and 6 (not shown), which suggests that the pair represents an oscillating statistical mode with a dominant period of 9 months. Also with the principal oscillation pattern analysis (Hasselmann 1988; Von Storch et al. 1995), we found a similar oscillatory mode (with a period of 9 months and a decay time of 11 months) in the interpolated dataset, and hence this statistical mode is quite robust in the data.

Figure 5 represents the anomaly patterns of RC 5–6, computed from the interpolated SSH dataset, for five phases during the oscillation. The starting time was chosen to be March 1995, when the amplitude of the statistical mode is quite large, and each subsequent picture is 1 month later showing nearly half of the cycle of the oscillation. One can see in Fig. 5 that the anomalies are concentrated around the mean axes of the Gulf Stream, the North Atlantic Current, and the Azores Current. After crossing the Southeast Newfoundland Ridge (at about 50°W) the Gulf Stream splits into two branches: the northern branch becomes the North Atlantic Current, and the southern one the Azores Current (e.g., see the review by Kaese and Krauss 1996). It is also evident that the anomalies are largest in the branching region. Moreover, there is an oscillation visible in the Gulf of Mexico. In Fig. 6, we show the propagating SSH anomalies associated with this RC pair along 35°N. A series of positive and negative anomalies propagates westward, that is, upstream, with an average velocity of about 5 cm s^{-1}. The zonal wavelength associated with this RC pair is on the order of 12.5°, which corresponds to 1138 km at 35°N.

Between 37° and 39°N, 65° and 60°W the New England Seamounts are situated and there seems to be interaction of the mode with this bottom topographic feature. This is in accordance with Lee and Cornillon (1996), who found that the 9-month period meanders, which are relatively barotropic, are affected by the sea-

←

FIG. 3. Reconstructed component (RC) pair 7–8 of Gulf Stream SST (K) describing the oscillating statistical mode having a 9-month time scale. The patterns are shown at a monthly interval, starting in Oct 1985, over one half-cycle of the oscillation; the other half-cycle is similar but with anomalies of reversed sign.

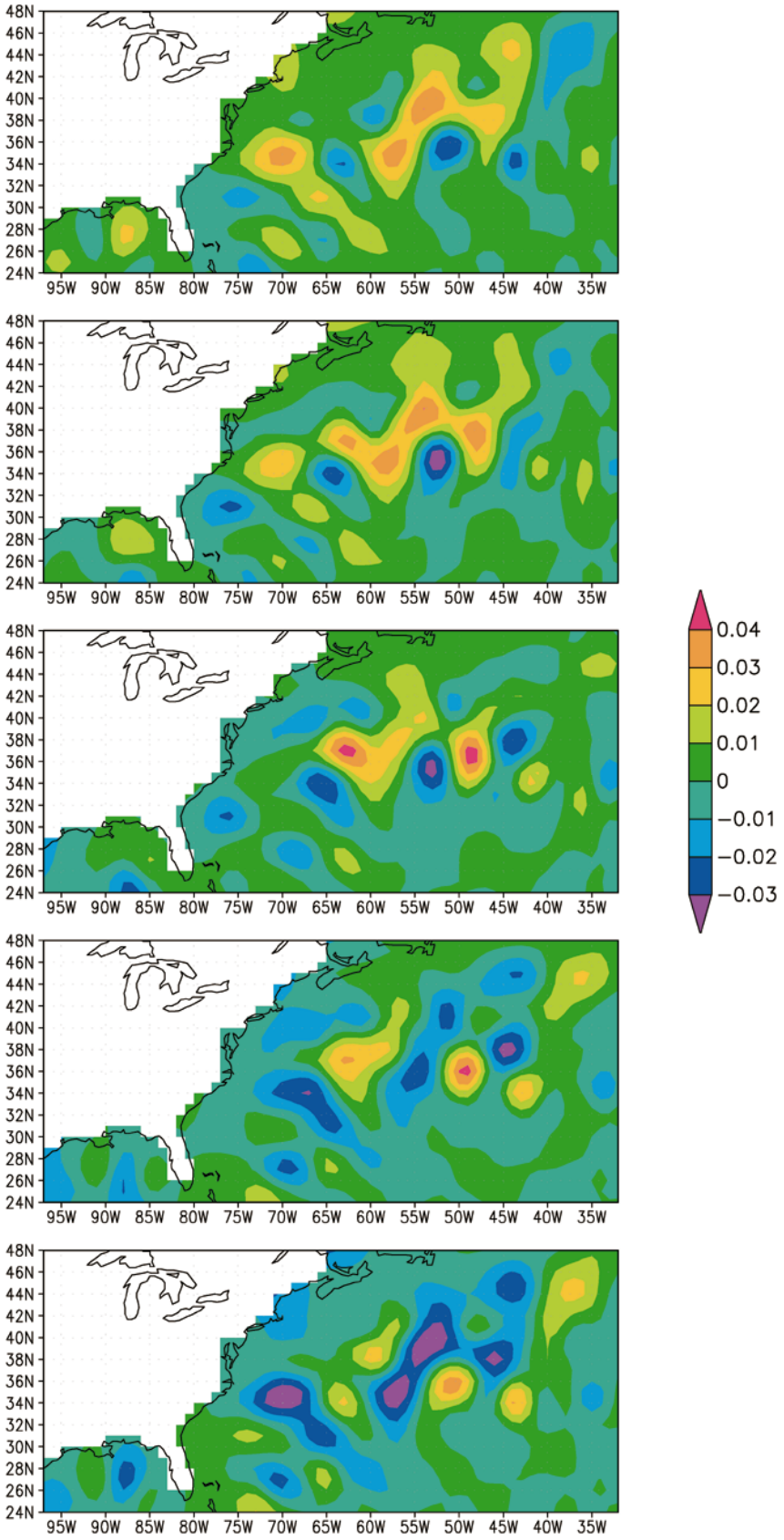
48N
46N
44N
42N
40N
38N
36N
34N
32N
30N
28N
26N
24N
95W 90W 85W 80W 75W 70W 65W 60W 55W 50W 45W 40W 35W
0.04
0.03
0.02
0.01
0
−0.01
−0.02
−0.03

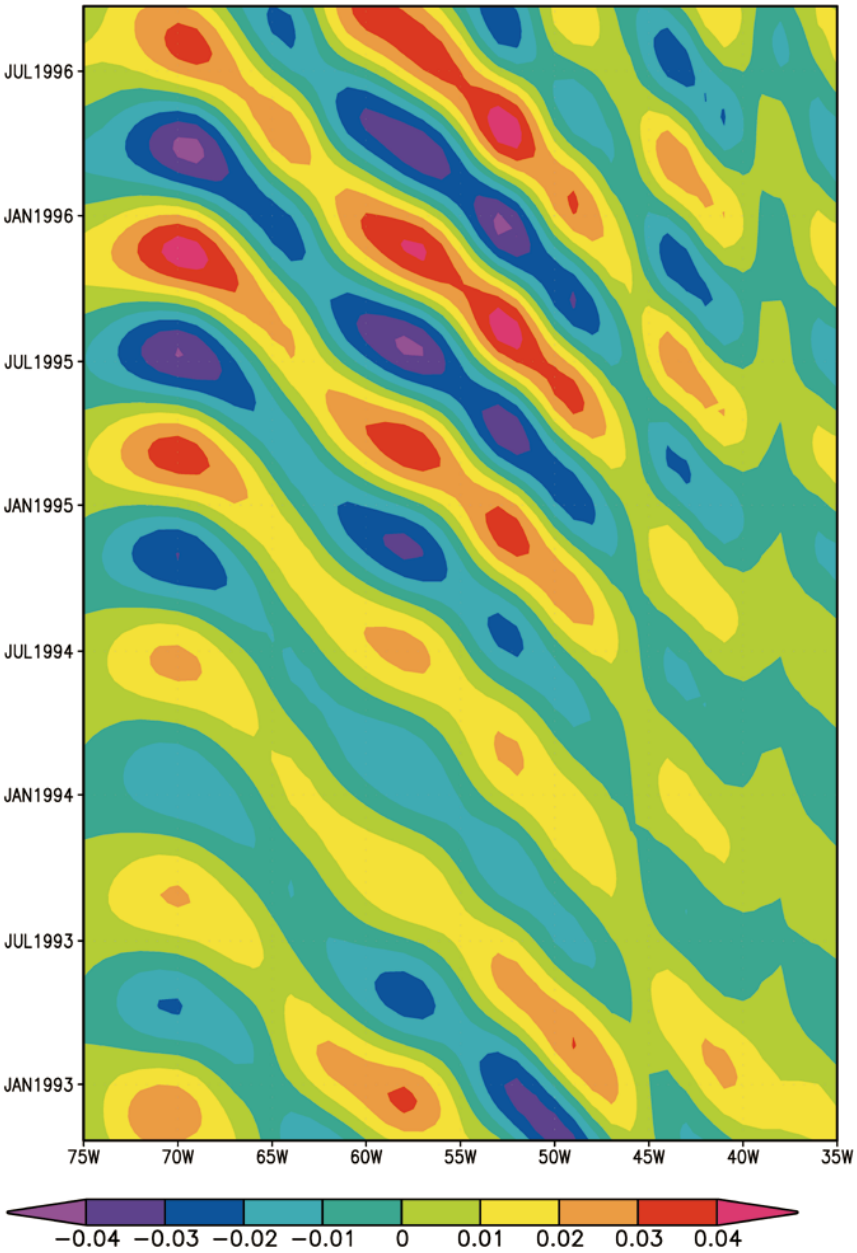

FIG. 6. Reconstructed component (RC) pair 5–6 of Gulf Stream SSH (m) describing the oscillating statistical mode having a 9-month time scale. The anomalies are shown along 35°N as a function of longitude and time.

mounts. Contrary to our result, however, they found a standing wave signature.

We can conclude that the spatial pattern of the reconstructed SSH anomalies of RC 5–6 (Fig. 5) is quite different from the spatial pattern of the reconstructed SST anomalies (Fig. 3), although the frequencies are the same. This motivates one to study whether there is any variability in both fields that appears to be related.

←

FIG. 5. Reconstructed component (RC) pair 5–6 of Gulf Stream SSH (m) describing the oscillating statistical mode having a 9-month timescale. The patterns are shown at a monthly interval, starting in Mar 1995, over one half-cycle of the oscillation; the other half cycle is similar but with anomalies of reversed sign.

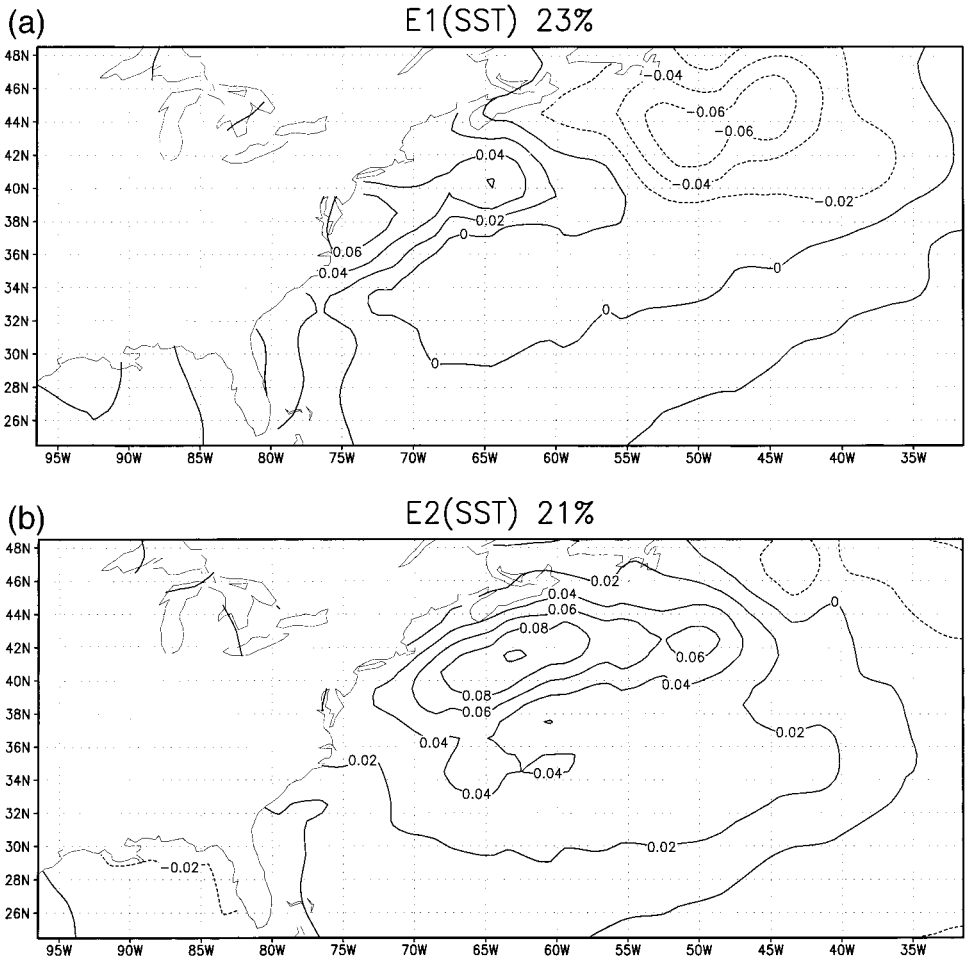

FIG. 7. The first two EOFs of nonseasonal Gulf Stream SST, namely (a) E1(SST) and (b) E2(SST), based on data for the period Nov 1992–Nov 1996. Negative contours are dashed. The fractions of variance of the data field explained by the respective PCs are indicated as well.

c. Covarying patterns in SST and SSH observations

To investigate whether the 9-month periodicities found in both SST and SSH are related, we investigated the coupled patterns of variability in both SST and SSH using the nonseasonal monthly mean datasets for the four years between November 1992 and November 1996 ($N = 48$). Now, M-SSA analysis is applied to the combined fields in order to find covarying propagating patterns in SST and SSH. To reduce the spatial dimensions, only the leading PCs of the separate PCA analyses, describing about 70% of the respective variances, are retained. These PCs, normalized by their singular values (in order that they contribute the same variance), provide the L input channels for the M-SSA algorithm. We have used a window length M of 16 months.

In this case the Monte Carlo significance test for M-SSA cannot be applied as the PCs of the two fields are not uncorrelated. The surrogate dataset would then be an L-channel multivariate AR(1) process, but it is inappropriate as a null hypothesis in a test for oscillatory behavior (Allen and Robertson 1996) because it can itself support oscillations. It was found that the first four ST–EOFs correspond to variations with long, unresolved timescales. The fifth and sixth ST–EOFs, however, constitute a pair of eigenfunctions with similar eigenvalues and enhanced variance on a timescale of 8 months. This pair explains 13% of the variance in the leading PCs, and ST–PC 5 and 6 are in quadrature as are the corresponding ST–EOF 5 and 6, which suggests that the pair represents an oscillating statistical mode with a dominant period of 8 months. The patterns and propagation of the reconstructed SSH anomalies of RC 5–6 are very similar to the ones found using the individual dataset (Figs. 5 and 6) and are therefore not shown. The SST anomaly pattern of RC 5–6 starts as a pattern very similar to the first EOF of SST, E1(SST) (Fig. 7a), and after one-quarter of a period the pattern is virtually E2(SST) (Fig. 7b). These patterns are different from the ones found using the individual dataset (Fig. 3), likely because of the use of a shorter time series.

This result contributes to the evidence of the existence of temporal variability with a dominant timescale of 8–9 months in the Gulf Stream area in accordance with earlier analyses (Lee and Cornillon 1995; Kelly et al. 1996). The mechanism of this variability is not easily extracted from the patterns of the eigenvectors of the (separate) M-SSA analyses. The spatial patterns found in SST and SSH do not look much alike. SST anomalies of opposite sign are oscillating around each other in the areas where meandering intensity is largest (Auer 1987). The SSH anomalies, which have smaller spatial scales than those of SST, are concentrated near the axes of the Gulf Stream, North Atlantic Current, and Azores Current and are propagating upstream. If one would look at only the patterns, it would not support any relationship between both fields. However, the combined M-SSA analysis suggests related physics causing the variability on this time scale in both fields. This is in accordance with Jones et al. (1998), who found that there is a relationship between SST and SSH anomalies in specific geographical regions associated with mesoscale variability. From the fact that these correlations are present at small and intermediate wavelengths, Jones et al. (1998) deduce that they are caused by large eddies, meanders, or Rossby waves rather than by the very large-scale seasonal response of the ocean to varying heat and water fluxes. In the next section, we investigate whether there is evidence of 9-month variability of the Gulf Stream in the POCM output.

d. Spatiotemporal variability of POCM fields

To determine properties of the vertical structure of the 9-month mode, if present in POCM, we have analyzed simulated temperature fields at two depth levels, namely 310 m (T310) and 610 m (T610). In order to facilitate the comparison to the SST and SSH observations, we have also used the SST and SSH fields from POCM. For a general comparison between POCM output and T/P data, the reader is referred to Stammer et al. (1996). The analysis has been performed for each field separately. In all cases, the nonseasonal anomalies were prefiltered with standard PCA and the leading PCs, which account for 80% of the variance, provide the L input channels for the M-SSA algorithm. We have obtained 19 years of data, so $N = 228$, and use a standard window length M of 76 months.

First, we show results from the M-SSA analysis of simulated SSH with $L = 21$. The result of the Monte Carlo significance test for M-SSA is shown for the data-adaptive basis in Fig. 8. Four data eigenvalue pairs, with associated periods of 18, 13, 9, and 5 months, are indicated as significant. The 9-month time scale belongs to a ST-PC pair that is in quadrature, which suggests that the pair represents an oscillating statistical mode.

The reconstructed anomaly patterns of SSH for this mode are shown in Fig. 9 for five phases during the oscillation. The starting time was chosen to be September 1980, when the amplitude of the statistical mode is quite large, and each subsequent picture is 1 month later showing nearly half of the cycle of the oscillation. The anomalies are clearly present in the Gulf Stream separation region and have a maximum amplitude of 8 cm. As in the case of the 9-month statistical mode from the T/P altimeter data, the anomalies are concentrated around the mean axis of the Gulf Stream and they are propagating upstream. However, the spatial scales of the simulated SSH anomalies are smaller than the scales of the observed SSH anomalies, which may just be a reflection of the T/P dataset's lower spatial resolution capability (Greenslade et al. 1997). The wavelength associated with the RC pair of the simulated SSH anomalies is about 500 km. The 13-month statistical mode from POCM SSH displays a spatial pattern similar to this 9-month statistical mode.

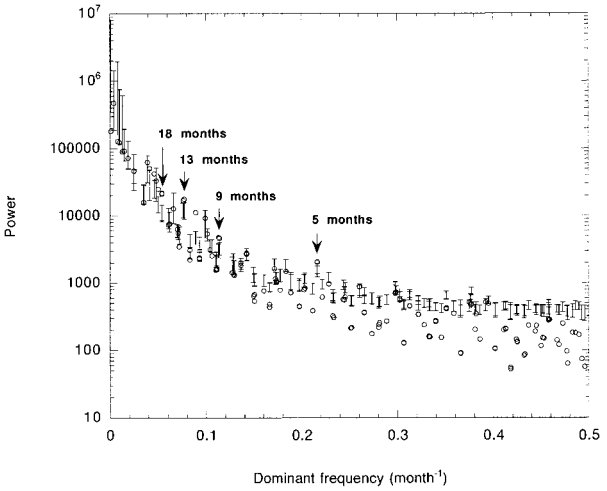

FIG. 8. Monte Carlo significance test of nonseasonal POCM SSH data in the Gulf Stream region for the period 1979–97, using $L = 21$ PCs from a conventional PCA as the input channels. Shown are projections of the SSH data onto the data-adaptive basis, similar to that in Fig. 1b, with a 76-month window ($M = 76$).

Secondly, we show results from the M-SSA analyses of T310 ($L = 11$) and T610 ($L = 20$). In both datasets, T310 and T610, there are statistically significant oscillating modes of variability with timescales of 20 and 13 months. Moreover, there is an oscillating mode of variability with a timescale of 9 months present in both datasets, which is not statistically significant at the 95% confidence level. However, because the other analyses described above indicated the 9-month timescale as statistically significant, and we are interested in the vertical structure of the 9-month mode, we have computed the reconstructed anomaly patterns of T310 and T610 for this mode. The results are shown in Fig. 10a for T310 and in Fig. 10b for T610. The spatial patterns of T310 and T610 are very similar to the pattern of SSH (cf. upper panel of Fig. 9) and a comparison of Figs. 10a and 10b indicates that the structure of the 9-month mode is approximately equivalent barotropic. The spatial pat-

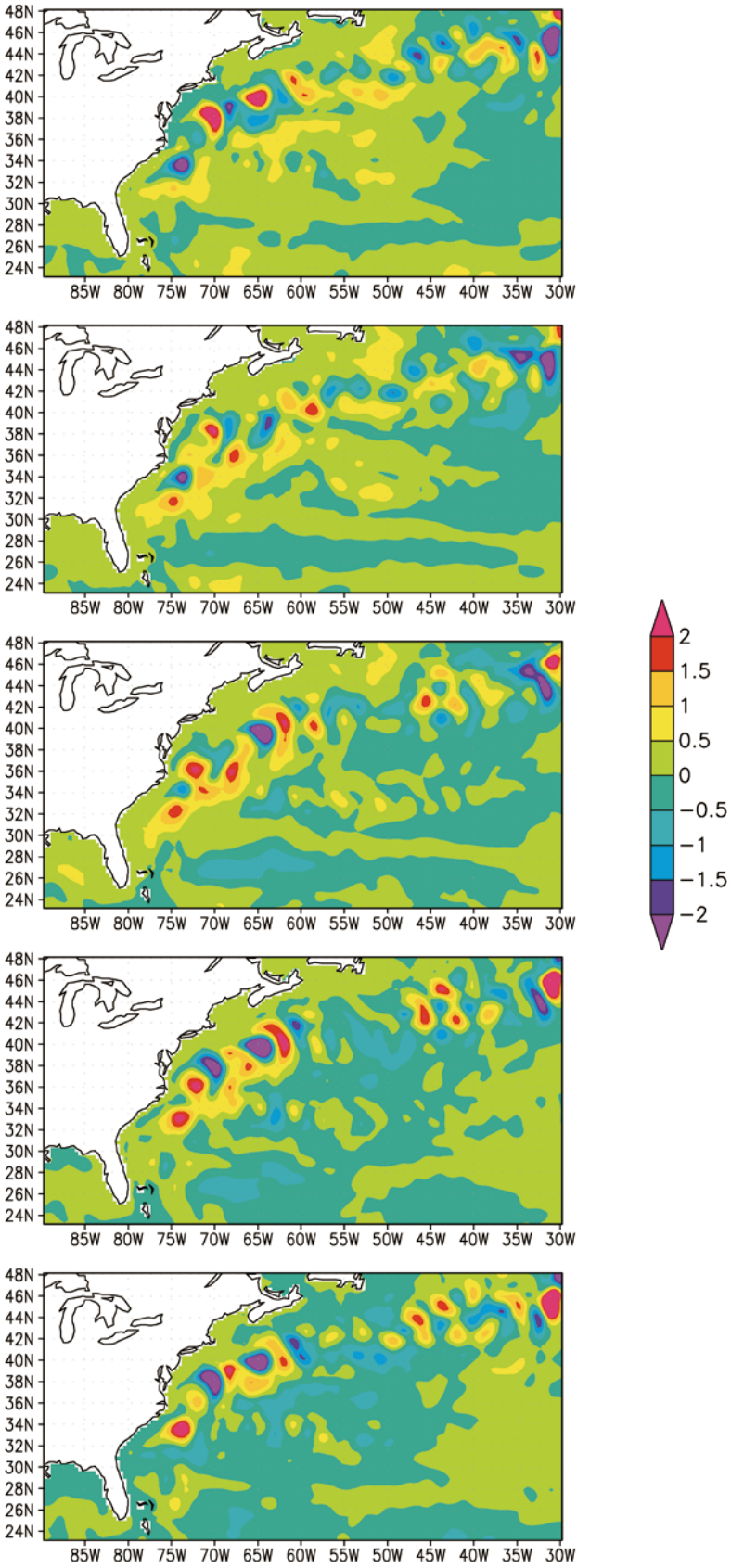
48N
46N
44N
42N
40N
38N
36N
34N
32N
30N
28N
26N
24N
85W 80W 75W 70W 65W 60W 55W 50W 45W 40W 35W 30W
2
1.5
1
0.5
0
−0.5
−1
−1.5
−2

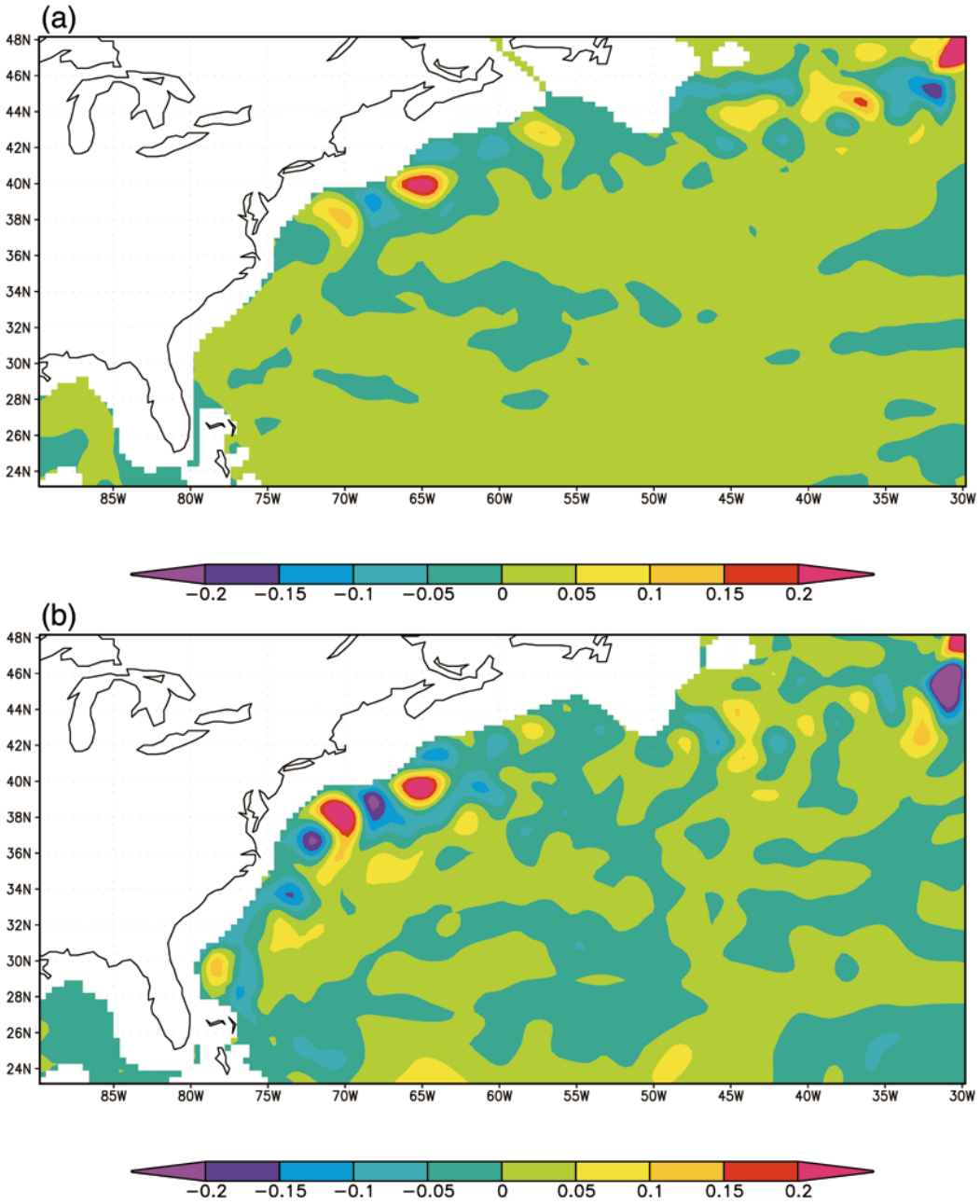

FIG. 10. Snapshot of the reconstructed component (RC) of Gulf Stream (a) T310 (K) and (b) T610 (K) from POCM describing the statistical mode having a 9-month time scale; the patterns are shown for Sep 1980.

terns of T310 and T610 for the 13- and 20-month statistical modes are very similar to the ones for the 9-month statistical mode. Indication of a 20-month timescale in observational data has been found by Speich et al. (1995) through spectral analysis of the Gulf Stream axis time series (their Fig. 18a). They derived this time series from the Comprehensive Ocean–Atmosphere Data Set (COADS) for the period 1970–92.

Finally, results are shown from the M-SSA analysis of simulated SST with $L = 25$. In this dataset there are

←

FIG. 9. Reconstructed component (RC) of Gulf Stream SSH (cm) from POCM describing the oscillating statistical mode having a 9-month timescale. The patterns are shown at a monthly interval, starting in Sep 1980, over one half cycle of the oscillation; the other half cycle is similar but with anomalies of reversed sign.

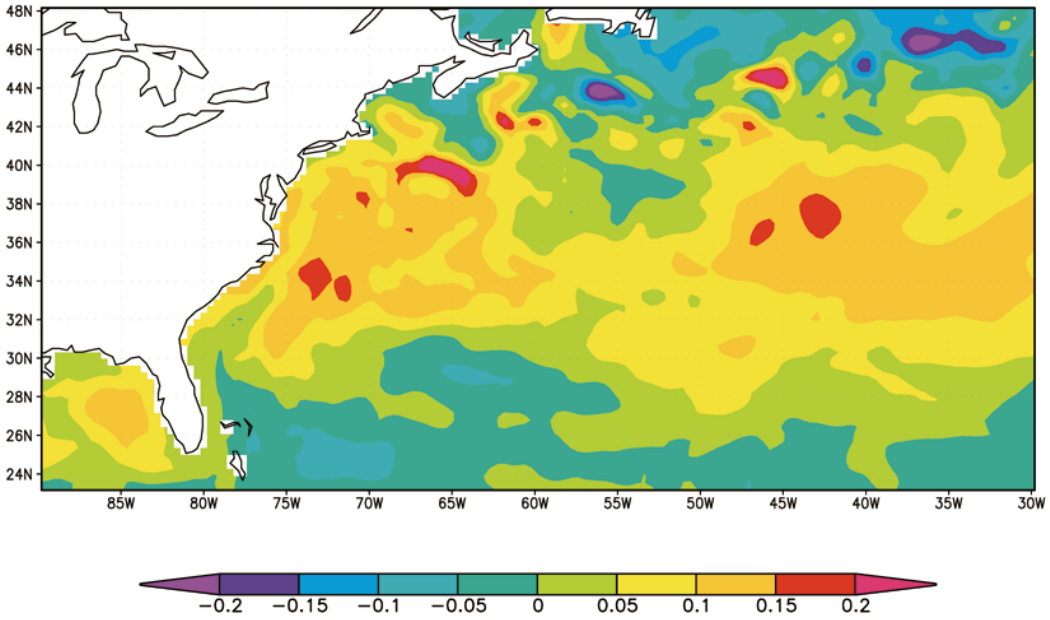

FIG. 11. Snapshot of the reconstructed component (RC) of Gulf Stream SST (K) from POCM describing the statistical mode having a 9-month timescale; the pattern is shown for Sep 1980.

also patterns of variability with timescales of 9 and 13 months present, which are, however, not statistically significant at the 95% confidence level. A snapshot of the reconstructed anomaly patterns of SST for the 9-month mode is shown in Fig. 11. The anomalies are largest around the mean Gulf Stream axis and have a maximum amplitude of 0.7 K. A comparison of Fig. 11 and the upper panel of Fig. 9 indicates that the spatial patterns of SST and SSH for the 9-month mode are quite different, although there is a correspondence with regard to the positive anomaly at (40°N, 65°W). The spatial pattern of the 13-month statistical mode in POCM SST (not shown) shows large-scale anomalies of opposite sign in the Gulf Stream separation region on the one hand and the extension region on the other hand. The Monte Carlo test of SST observations gives an indication of variability on a time scale of 14 months (see Fig. 1b), and the associated pattern of variability consists also of large spatial scales.

From the results of the M-SSA analyses described above, we can conclude that the connection between the spatial patterns of SST and SSH for the 9- and 13-month statistical modes is also unclear in the POCM output. In Table 3 the results of the M-SSA analyses of the POCM output and of the observations have been summarized. In the next section, we explore whether internal ocean dynamics may be the source of the 9-month variability in the Gulf Stream region.

4. Spatiotemporal variability within a barotropic shallow-water model

This study extends that in Dijkstra and Molemaker (1999), where successive bifurcations of the wind-driven ocean circulation were studied within a 1.5-layer shallow-water (SW) model on a β plane. In the model below, the full North Atlantic basin (10°–65°N, 85°–5°W) is considered using realistic geometry and windstress forcing (Trenberth et al. 1989) but no bottom topography, and only the barotropic circulation is considered.

a. Formulation

Consider a flat-bottomed ocean basin with a realistic horizontal domain, $\mathcal{V}$, and bounded by a closed contour Γ. The density of the ocean is constant and the flow is driven by a windstress $\tau(\phi, \theta) = \tau_0(\tau^\phi, \tau^\theta)$, where τ_0 is the amplitude and (τ^ϕ, τ^θ) provides the spatial pattern. Lateral friction, with lateral friction coefficient A_H,

TABLE 3. Summary of common time scales T detected in the POCM output (P) and in the observations (O).

T (months)	SSH_P	T310_P	T610_P	SST_P	SST_O	SSH_O
9	*	*	*	*	*	*
13	*	*	*	*	*	
20		*	*		Speich et al. (1995)	

is the dissipative mechanism in the model. In the usual notation, the velocities in eastward and northward directions are indicated by u and v, respectively and h is the thickness of the water column (with equilibrium value D), and changes due to changes in the sea surface height. The governing shallow-water equations are nondimensionalized using scales r_0, D, U, r_0/U and τ_0 for length, layer depth, velocity, time, and windstress, respectively, where r_0 is the radius of the earth, and become

$$\epsilon\left(\frac{\partial u}{\partial t} + \frac{u}{\cos\theta}\frac{\partial u}{\partial \phi} + v\frac{\partial u}{\partial \theta} - uv\tan\theta\right) - v\sin\theta = -\frac{\epsilon F}{\cos\theta}\frac{\partial h}{\partial \phi} + E\left(\nabla^2 u - \frac{u}{\cos^2\theta} - \frac{2\sin\theta}{\cos^2\theta}\frac{\partial v}{\partial \phi}\right) + \alpha\frac{\tau^\phi}{h} \quad (4a)$$

$$\epsilon\left(\frac{\partial v}{\partial t} + \frac{u}{\cos\theta}\frac{\partial v}{\partial \phi} + v\frac{\partial v}{\partial \theta} + u^2\tan\theta\right) + u\sin\theta = -\epsilon F\frac{\partial h}{\partial \theta} + E\left(\nabla^2 v - \frac{v}{\cos^2\theta} + \frac{2\sin\theta}{\cos^2\theta}\frac{\partial u}{\partial \phi}\right) + \alpha\frac{\tau^\theta}{h} \quad (4b)$$

$$\frac{\partial h}{\partial t} + \frac{1}{\cos\theta}\left(\frac{\partial (hu)}{\partial \phi} + \frac{\partial (hv\cos\theta)}{\partial \theta}\right) = 0. \quad (4c)$$

On the boundary Γ of the domain no-slip conditions are prescribed; that is,

$$(\phi, \theta) \in \Gamma : u = v = 0. \quad (5)$$

The parameters in these equations are the Rossby number ϵ, the Froude number F, the Ekman number E, and the windstress coefficient α. Expressions for these parameters are

$$\epsilon = \frac{U}{2\Omega r_0}; \qquad F = \frac{gD}{U^2}; \qquad E = \frac{A_H}{2\Omega r_0^2};$$

$$\alpha = \frac{\tau_0}{2\Omega\rho DU}, \quad (6)$$

where Ω is the angular velocity of the earth. Standard values of the parameters in this model are listed in Table 4.

b. Numerical methods

Within the SW model, a finite difference discretization was used on the domain [10°N, 65°N] × [85°W, 5°W] with a resolution of 0.5° × 0.5°. Continental geometry and boundary conditions are taken into account by first discretizing the equations on the sphere and then substituting equations with boundary conditions, according to whether the point is a land point or an ocean point.

Steady-state solutions lead to a set of nonlinear algebraic equations of the form

$$\mathbf{F}(\mathbf{u}, \mathbf{p}) = 0. \quad (7)$$

Here $\mathbf{u}$ is a d-dimensional vector consisting of the unknowns at the grid points, $\mathbf{p}$ is the p-dimensional vector of parameters, and $\mathbf{F}$ is a nonlinear mapping from $R^d \times R^p \to R^d$, where d indicates the number of degrees of freedom. To determine branches of steady solutions of the Eq. (7) as one of the parameters (say μ) is varied, the pseudo-arclength method is used. The branches $[\mathbf{u}(s), \mu(s)]$ are parameterized by an ''arclength'' parameter s. An additional equation is obtained by ''normalizing'' the tangent

$$\dot{\mathbf{u}}_0^T(\mathbf{u} - \mathbf{u}_0) + \dot{\mu}_0(\mu - \mu_0) - \Delta s = 0, \quad (8)$$

where $(\mathbf{u}_0, \mu_0)$ is an analytically known starting solution or a previously computed point on a particular branch and Δs is the steplength.

To calculate a steady-state solution of the system of equations (7) an extra condition for h is required to regularize the equations, since h is determined up to an additive constant. This is done by an integral condition for h over the domain $\mathcal{V}$ that removes the ambiguity from the layer depths; that is,

$$\int_{\mathcal{V}} h\cos\theta\, d\phi\, d\theta = |\mathcal{V}|, \quad (9)$$

which is an expression of conservation of mass of the layer. The integral is equal to $|\mathcal{V}|$, the (dimensionless) area of the domain since the layer depth is scaled with D. In models that integrate the equations in time, this regularization problem is absent since the integral of the layer depth is set by the initial conditions.

When a steady state is determined, the linear stability of the solution is considered and transitions that mark qualitative changes such as transitions to multiple equilibria (pitchfork bifurcations or limit points) or periodic behavior (Hopf bifurcations) can be detected. The linear stability analysis amounts to solving a generalized eigenvalue problem of the form

$$\mathbf{A}\mathbf{x} = \sigma\mathbf{B}\mathbf{x}, \quad (10)$$

where $\mathbf{A}$ and $\mathbf{B}$ are nonsymmetric matrices. Bifurcations are detected from crossings of σ with the imaginary axis. Solution techniques for these problems are presented in Dijkstra et al. (1995).

TABLE 4. Standard values of parameters in the barotropic SW model.

Parameter	Value	Parameter	Value
Dimensional parameters			
r_0	6.37×10^6 m	τ_0	1.5×10^{-1} Pa
D	1.0×10^3 m	A_H	2.0×10^2 m^{2}s^{-1}
g	9.8 ms^{-2}	U	1.0×10^{-1} ms^{-1}
ρ	1.0×10^3 kgm^{-3}	Ω	7.3×10^{-5} s^{-1}
Dimensionless parameters			
α	1.0×10^{-2}	E	3.4×10^{-8}
ϵ	1.1×10^{-4}	F	9.8×10^5

c. Results

The bifurcation diagram is shown in Fig. 12a using the Ekman number E as control parameter and fixing all other parameters as in Table 4; it consists of a perturbed pitchfork bifurcation (Golubitsky and Schaeffer 1985). On the vertical axis, the maximum northward volume transport Φ (in Sv) over a section is shown, which is calculated as

$$\Phi = (UDr_0) \max \int_{\phi_W}^{\phi_E} vh \cos\theta \, d\phi, \qquad (11)$$

where the maximum is taken both over ϕ and θ. An important result is the existence of multiple equilibria, just as in the 1.5-layer SW model on a β plane (Dijkstra and Molemaker 1999). Two solution branches are found, on which solutions are unstable for $E < 2.5 \times 10^{-7}$. A solution on the lower branch is shown as a contour plot of h for $E = 1.6 \times 10^{-7}$ in Figs. 12b and 12d. It displays the double gyre circulation, typical for the North Atlantic Ocean with a ''deflected'' Gulf Stream that separates too far north compared to reality. The small recirculation gyre in the separation region reflects the inability of the flow to rejoin the Sverdrup interior immediately. It first has to get rid of its excess vorticity by recirculating several times. Moreover, there is a weak southern recirculation cell and at this value of E the transport Φ is about 46 Sv. This solution resembles very much the mean SSH field from POCM in the Gulf Stream region (cf. Fig. 14 in Semtner and Chervin 1992). Thus, POCM also shows a Gulf Stream that separates too far north.

The other branch exists only for $E < 2.2 \times 10^{-7}$, which is the position of the limit point on this branch. The solution at $E = 1.6 \times 10^{-7}$ (Figs. 12c and 12e) displays a ''separated'' Gulf Stream that actually seems to separate twice. First, it separates too far south compared to reality, and later on it separates too far north (at about the same latitude as in Fig. 12d). There is now a strong southern and a weak northern recirculation cell. At this value of E, the transport Φ is about 70 Sv, which is 1.5 times larger than that in Fig. 12b and somewhat larger than current estimates near Cape Hatteras of about 50–65 Sv (Johns et al. 1995). By comparing Figs. 12b and 12c, it can be concluded that the circulation patterns outside the region of the western boundary current are very similar so that the multiple equilibria are related to the different separation structures of the Gulf Stream.

We have also computed the local vorticity balances for the multiple equilibria. Outside the western boundary layers the Sverdrup balance holds for both equilibria. For the deflected Gulf Stream the boundary layer is of the nonlinear Munk type, and for the separated Gulf Stream the boundary layer is highly nonlinear, with lateral friction playing a minor role.

On the lower branch in Fig. 12a, a Hopf bifurcation occurs at $E = 2.5 \times 10^{-7}$ and is marked with H_1. The steady state at this value of E is similar to Fig. 12b and therefore not shown. At H_1 the steady state becomes unstable to one oscillating dynamical mode. The pattern of this mode is determined from the eigenvector $\mathbf{x} = \mathbf{x}_r + i\mathbf{x}_i$ associated with the eigenvalue $\sigma = \sigma_r + i\sigma_i$ in (10). These span an oscillatory mode given by

$$\mathbf{\Psi}(t) = \exp(\sigma_r t)\{\cos(\sigma_i t)\mathbf{x}_r - \sin(\sigma_i t)\mathbf{x}_i\} \qquad (12)$$

with dimensional period $T = 2\pi r_0/(U\sigma_i)$. The perturbation is shown at four phases within half a period of the oscillation in Figs. 13a–d. The dynamical mode is located around the axis of the western boundary current and propagates southwestward, that is, upstream. It has a period of 6 months, and a wavelength of about 550 km. From Figs. 12d and 13a–d we can deduce that the perturbation adds cross-stream components to the flow in the western boundary current; that is, it causes the Gulf Stream to meander.

To investigate the sensitivity of the results to the layer thickness D, we have computed a regime diagram separating steady from oscillatory behavior (Fig. 14a). At each value of D, the linear stability boundary is determined by the value of E at the Hopf bifurcation H_1. It is obvious from Fig. 14a that the circulation gets more stable as D increases. This is a result of the fact that the same energy input by the windstress forcing is distributed over a deeper layer, which stabilizes the flow. The spatial pattern of the neutral mode does not change much with D, but the period of the oscillation increases from 6 to 11 months in the range of D considered (Fig. 14b). Of course, the average depth of the real Gulf Stream region depends on the domain chosen, but values slightly larger than 1 km do seem to be reasonable. Inclusion of bottom topography could change this mode and period substantially, but it has a large effect on the sea surface height in a barotropic model and hence it was not considered here.

A second Hopf bifurcation (H_2) occurs at $E = 2.1 \times 10^{-7}$ on the branch of the separated Gulf Stream solution (Fig. 12a). The period of this oscillation is 2 months. The transition structure of the perturbation is shown in Figs. 15a–d, with the basic state being similar to that in Fig. 12c. Its maximum response is found in the high shear region to the southeast of Greenland, the propagation direction is westward and the perturbations have

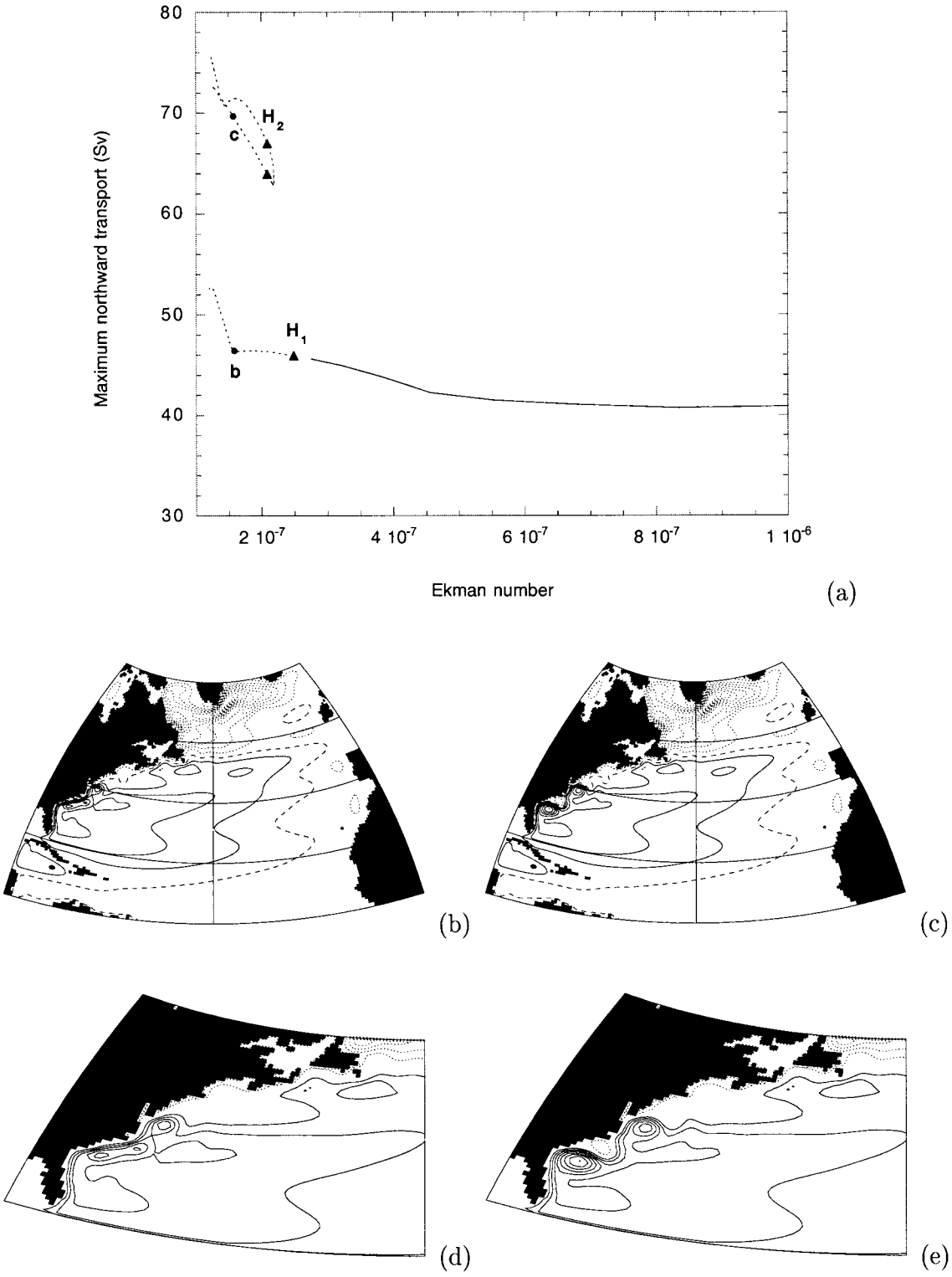

FIG. 12. (a) Bifurcation diagram with the Ekman number as control parameter. Drawn (dotted) branches indicate stable (unstable) steady states, whereas the Hopf bifurcation points are indicated by triangles. The intersection of the upper branch does not indicate a bifurcation; it is due to the choice of norm. (b) Contour plot of the layer thickness anomaly for the ''deflected'' Gulf Stream at $E = 1.6 \times 10^{-7}$. The contour levels are scaled with respect to the maximum value of the field. (c) Contour plot of the layer thickness anomaly for the 'separated' Gulf Stream at $E = 1.6 \times 10^{-7}$. (d) Detail of (b). (e) Detail of (c).

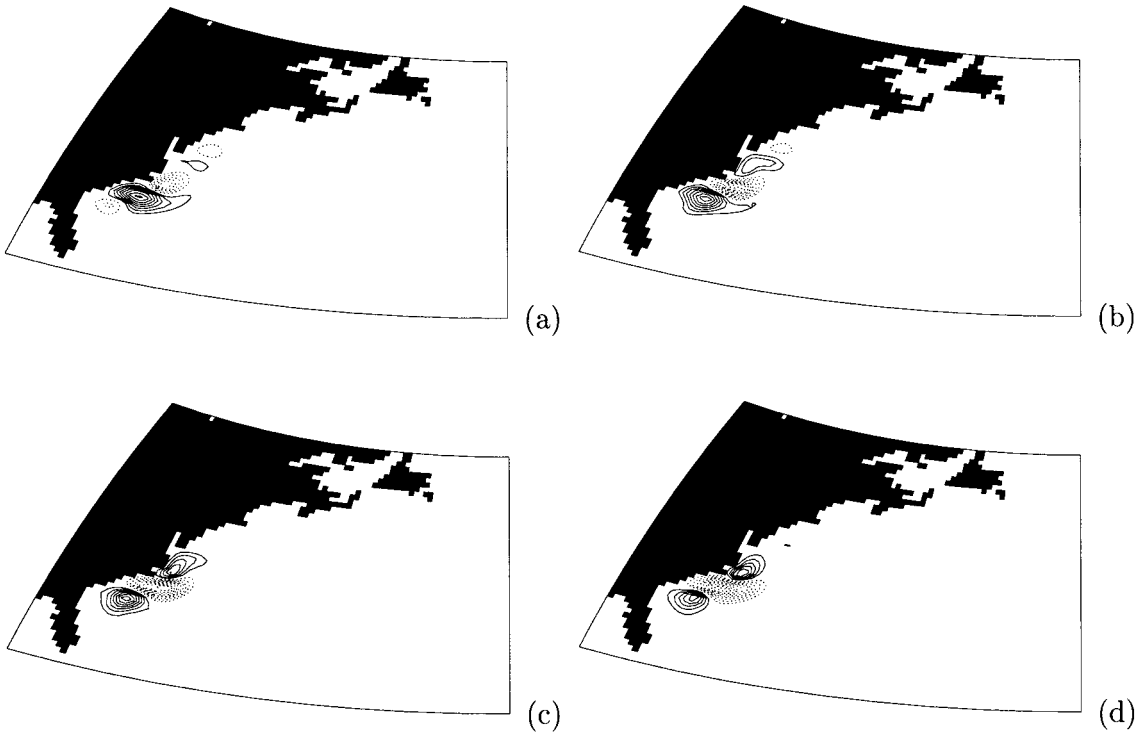

FIG. 13. Contour plot of the layer thickness anomaly of the transition structure [(a)–(d)] of the neutral mode at the Hopf bifurcation H_1 in Fig. 12a at several phases of the oscillation. (a) $\sigma_i t = 0$; (b) $\sigma_i t = \pi/4$; (c) $\sigma_i t = \pi/2$; (d) $\sigma_i t = 3\pi/4$.

a typical wavelength of 500 km. The relevance of this dynamical mode to the variability in the northern part of the Atlantic basin is not further considered.

5. Discussion

As mentioned in the introduction, focus of this work was to find a plausible physical mechanism of the near-annual variability of the Gulf Stream near its separation location. Both the M-SSA analyses of the individual fields of SST and SSH observations clearly give a statistically significant mode of variability having a time scale of 9 months. This type of variability is very unlikely to be caused by red noise processes (Hasselmann 1976). With the fact that this time scale of variability has also been found in other studies (Lee and Cornillon

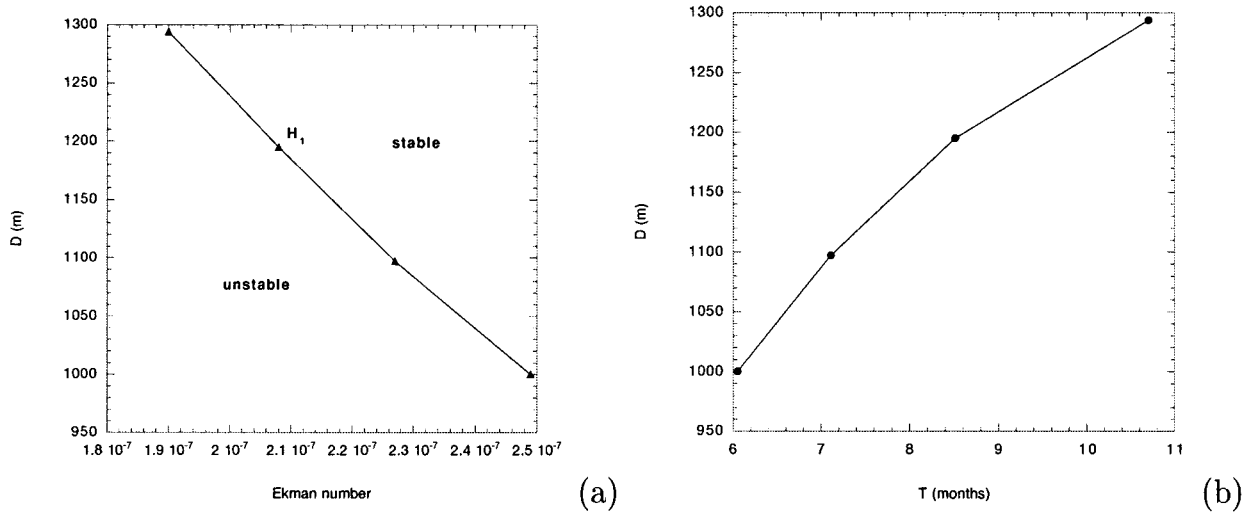

FIG. 14. (a) Path of the first Hopf bifurcation H_1 (as in Fig. 12a), that is, the linear stability boundary, in the (E, D) plane. (b) Oscillation period (T) of the neutral mode at H_1 as a function of the layer thickness D.

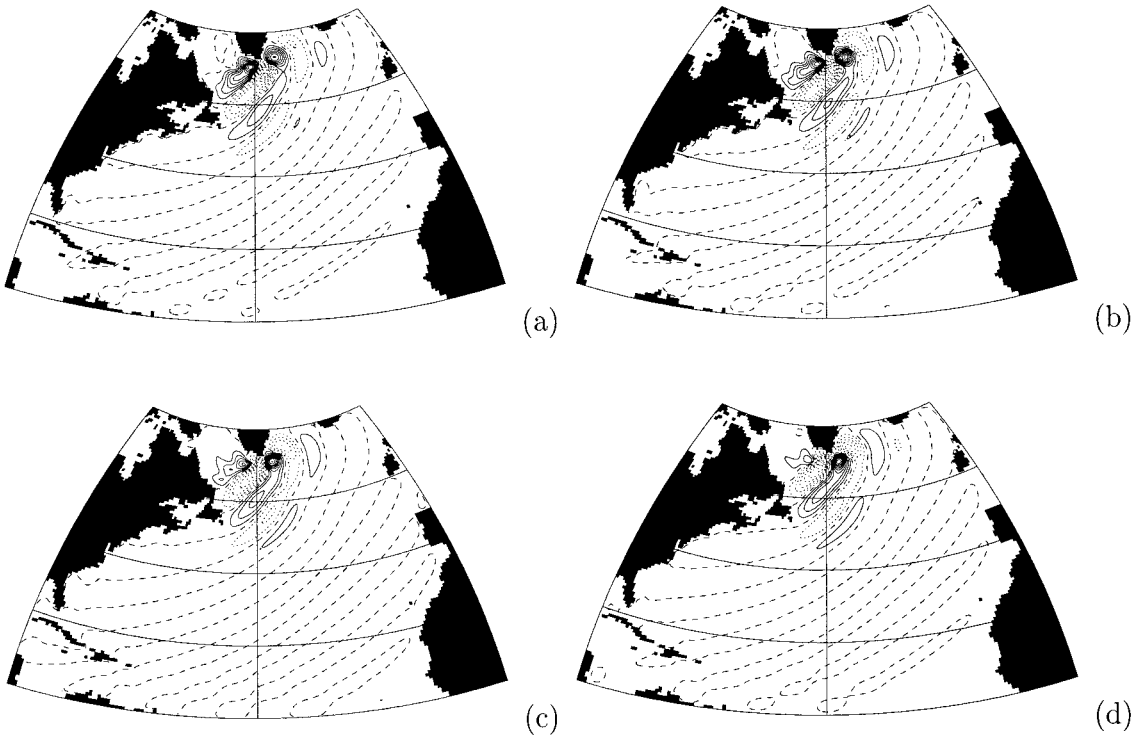

FIG. 15. Contour plot of the layer thickness anomaly of the transition structure [(a)–(d)] of the neutral mode at the Hopf bifurcation H_2 in Fig. 12a at several phases of the oscillation. (a) $\sigma_i t = 0$; (b) $\sigma_i t = \pi/4$; (c) $\sigma_i t = \pi/2$; (d) $\sigma_i t = 3\pi/4$.

1995), we conclude that there is dominant variability on a 9-month timescale in the Gulf Stream separation region.

However, the patterns of both SST and SSH of this statistical mode have no direct correspondence. Large-scale SST anomalies are found over most of the basin with some hardly identifiable pattern of rotating anomalies in the Gulf Stream separation region. The SSH anomalies are of smaller scale, but they are present with comparable amplitude over the whole region. Although the combined M-SSA analysis shows that the statistical modes of both SST and SSH on the intermonthly timescale may be related, the physical connection between both fields is not clear. This is partly due to the statistical techniques themselves because the statistically significant modes are not the patterns with highest variance and are therefore subjected to orthogonality constraints that may blur the connection between the pattern and the physics causing it.

M-SSA analysis of the POCM output also shows variability on a timescale of 9 months. Moreover, statistically significant modes with timescales of 13 and 20 months have been detected in the POCM output. Indication of a 14-month timescale has been found in the SST observations (Fig. 1b) and a 20-month timescale has been detected by Speich et al. (1995) in the COADS dataset. The connection between SST and SSH for the 9- and 13-month statistical modes turned out to be unclear for both observations and POCM, as far as detected. As there is only a very weak restoring of POCM SST, the reason for this vague connection may be the same for both observations and POCM. In the future this connection may be studied in the framework of the shallow-water model by adding a surface mixed layer. Analysis of the POCM temperature fields at several vertical levels has clearly demonstrated that the structure of the 9, 13, and 20 month modes is approximately equivalent barotropic. Therefore, it seems legitimate to investigate the hypothesis of this paper, put forward in the introduction, in a barotropic model.

The shallow-water model used to study the transition to time dependence of wind-driven flows suffers from severe simplifications by being fully barotropic and discarding any effect of bottom topography. On the other hand, until now it is the most realistic model on which techniques of bifurcation analysis have been applied. As in previous studies (Dijkstra and Katsman 1997; Dijkstra and Molemaker 1999), two mean flow patterns of the Gulf Stream are found of which the origin was discussed at length in Dijkstra and Molemaker (1999). These flows only differ with respect to their separation behavior near the North American coast, while being the same over the remainder of the basin.

The first oscillating dynamical mode to become unstable has a timescale on the order of months and is about 9 months for an average depth of the basin of 1200 m. Its perturbation pattern is localized in the recirculating cells, with very small amplitude over the

remainder of the basin, and it causes the mean flow to meander. The origin of this mode seems to be related to the ocean basin modes found in a 1.5-layer QG model (Dijkstra and Katsman 1997). Dijkstra and Molemaker (1999) have followed the latter modes through a hierarchy of 1.5-layer QG and SW models and found that the modes remained closely related. Therefore, the propagation mechanism of the oscillatory instability is similar to that of free Rossby waves, while the growth of the perturbation is related to the horizontal shear strength within the western boundary current (Dijkstra and Katsman 1997). We will refer to this dynamical mode as the barotropic western boundary current (BWBC) mode below.

In the region of the Gulf Stream common features of the 9-month mode in POCM and the BWBC mode are that they both have a (near) barotropic structure, have similar timescales, and that the anomalies have wavelengths of about 500 km, are propagating upstream, and are concentrated around the mean axis of the Gulf Stream. Therefore, it is plausible that the 9-month mode in POCM (e.g., Fig. 9) is similar to the BWBC mode (Fig. 13). The connection with the observations is less obvious, as the spatial patterns of the SST and SSH modes do not correspond to the spatial pattern of the BWBC mode. They do, however, have a similar time scale of propagation. Besides, the anomalies of the SSH mode are also propagating upstream, and are concentrated around the mean axis of the Gulf Stream. However, it is impossible to claim that the physics of the BWBC mode is that causing the variability in the SST and SSH observations on that time scale. Instead, we claim something weaker, that is, that the BWBC mode contributes to the significance of the variability on this time scale, even if the dominant physics controlling the variability would be caused by other processes (neglected in the SW model).

Other studies have strongly suggested that the 9-month variability is not related to variations in external forcing, such as the surface heat flux (Kelly et al. 1996) and that internal ocean dynamics is the most likely process to drive these changes in the flow field. The BWBC mode destabilizes the idealized Gulf Stream, which means that this perturbation pattern is able to extract energy out of the mean flow on this particular timescale. Hence, the energy level of this frequency can be easily increased due to the barotropic instability mechanism. Consequently, even if the physics of the variability is not caused by the BWBC mode, this mode may still contribute to its significance because it enhances the variance on this timescale in a totally different way as red noise processes would.

Suppose, on the other hand, that the underlying physics of this variability is indeed caused by the BWBC mode, then the question is why the statistical techniques do not find the pattern of this mode. That the spatial patterns of the dominant significant M-SSA modes in the SST and SSH observations and the BWBC mode in the SW model do not look alike may be explained by the property of M-SSA that it is able to discriminate between two oscillations with the same period only if they have spatially orthogonal patterns (Plaut and Vautard 1994). Apart from the orthogonality contraints in the patterns as mentioned above, there are many processes contributing to the energy level on the particular timescale. Nonlinear interaction of baroclinic instabilities (which are modes of shorter timescale) can easily give a contribution on this timescale as can variations in atmospheric forcing. The statistical techniques, which are all in some way variance maximizing, pick up these signals and hence the resulting pattern on this timescale will show signatures not related to the main cause of the variability. If there were no clear non-red-noise-like source of energy at the particular frequency, as present here due to the BWBC mode, the pattern of the statistically determined patterns would likely not be significant. Hence, even though the significance is induced by the presence of the BWBC mode, the statistical technique would not be able to find its correct pattern.

With this argumentation, there is good reason to conjecture that the 9-month variability of the Gulf Stream is caused by a barotropic instability of the mean Gulf Stream path near its separation. Confirmation of this conjecture has been obtained through the connection between the 9-month mode from the POCM output and the BWBC mode in the SW model. This conjecture can be rejected if it turns out that stratification and other factors cause the BWBC mode, found here, to disappear. Future research along this path will concentrate to determine the internal modes of variability in more realistic models and determine their contribution in transient simulations of the ocean circulation.

Acknowledgments. This work was supported by the Netherlands Organization for Scientific Research (NWO) under a PIONIER grant to HD. All computations were performed on the CRAY C90 at the Academic Computing Centre (SARA), Amsterdam, the Netherlands, within the project SC498. Use of these computing facilities was sponsored by the National Computing Facilities Foundation with financial support from NWO. The authors thank Robin Tokmakian (NPS, USA) for supplying the POCM output, Andy Robertson (UCLA, USA) for providing the M-SSA software, Jeroen Molemaker (IMAU, NL) for developing the SW model, Frank Selten (KNMI, NL) for supplying data analysis software, and Femke Vossepoel (TU Delft, NL) and Mathijs Schouten (IMAU, NL) for providing the interpolation software for the TOPEX/Poseidon data. Furthermore, the authors thank both anonymous reviewers for their useful comments.

REFERENCES

Allen, M. R., and A. W. Robertson, 1996: Distinguishing modulated oscillations from coloured noise in multivariate datasets. *Climate Dyn.,* **12,** 775–784.

Auer, S. J., 1987: Five-year climatological survey of the Gulf Stream system and its associated rings. *J. Geophys. Res.,* **92,** 11 709–11 726.

Cessi, P., and G. R. Ierley, 1995: Symmetry-breaking multiple equilibria in quasigeostrophic, wind-driven flows. *J. Phys. Oceanogr.,* **25,** 1196–1205.

Dijkstra, H. A., and C. Katsman, 1997: Temporal variability of the wind-driven quasi-geostrofic double gyre ocean circulation: Basic bifurcation diagrams. *Geophys. Astrophys. Fluid Dyn.,* **85,** 195–232.

——, and M. J. Molemaker, 1999: Imperfections of the North-Atlantic wind-driven ocean circulation: Continental geometry and wind-stress shape. *J. Mar. Res.,* **57,** 1–28.

——, ——, A. J. Van der Ploeg, and E. F. F. Botta, 1995: An efficient code to compute nonparallel flows and their linear stability. *Comput. Fluids,* **24,** 415–434.

Fuglister, F. C., 1972: Cyclonic rings formed by the Gulf Stream 1965–1966. *Studies in Physical Oceanography,* A. L. Gordon, Ed., Vol. 1, Gordon and Breach, 137–168.

Golubitsky, M., and D. Schaeffer, 1985: *Singularities and Groups in Bifurcation Theory.* Springer-Verlag, 533 pp.

Greenslade, D., D. Chelton, and M. Schlax, 1997: The midlatitude resolution capability of sea level fields constructed from single and multiple satellite altimeter datasets. *J. Atmos. Oceanic Technol.,* **14,** 849–870.

Hall, M., and N. Fofonoff, 1993: Downstream development of the Gulf Stream from 68° to 55°W. *J. Phys. Oceanogr.,* **23,** 225–249.

Hansen, D., 1970: Gulf Stream meanders between Cape Hatteras and the Grand Banks. *Deep-Sea Res.,* **17,** 495–511.

Hasselmann, K., 1976: Stochastic climate models. Part I. Theory. *Tellus,* **28,** 473–485.

——, 1988: PIPs and POPs: The reduction of complex dynamical systems using principal interaction and oscillation patterns. *J. Geophys. Res.,* **93,** 11 015–11 021.

Jiang, S., F. Jin, and M. Ghil, 1995: Multiple equilibria and aperiodic solutions in a wind-driven double gyre, shallow water model. *J. Phys. Oceanogr.,* **25,** 764–786.

Johns, W., T. Shay, J. Bane, and D. Watts, 1995: Gulf Stream structure, transport and recirculation near 68°W. *J. Geophys. Res.,* **100,** 817–838.

Jones, M., M. Allen, T. Guymer, and M. Saunders, 1998: Correlations between altimetric sea surface height and radiometric sea surface temperature in the South Atlantic. *J. Geophys. Res.,* **103,** 8073–8087.

Kaese, R. H., and W. Krauss, 1996: The Gulf Stream, the North Atlantic Current, and the origin of the Azores Current. *The Warmwatersphere of the North Atlantic Ocean,* W. Krauss, Ed., Borntraeger, 291–337.

Katsman, C., H. Dijkstra, and S. Drijfhout, 1998: The rectification of wind-driven flow due to its instabilities. *J. Mar. Res.,* **56,** 559–587.

Kelly, K. A., M. J. Caruso, S. Singh, and B. Qiu, 1996: Observations of atmosphere–ocean coupling in midlatitude western boundary currents. *J. Geophys. Res.,* **101,** 6295–6312.

——, S. Singh, and R. Huang, 1999: Seasonal variations of sea surface height in the Gulf Stream region. *J. Phys. Oceanogr.,* **29,** 313–327.

Lee, T., and P. Cornillon, 1995: Temporal variation of meandering intensity and domain-wide lateral oscillations of the Gulf Stream. *J. Geophys. Res.,* **100** (C7), 13 603–13 613.

——, and ——, 1996: Propagation and growth of Gulf Stream meanders between 75° and 45°W. *J. Phys. Oceanogr.,* **26,** 225–241.

Maul, G., P. DeWitt, A. Yanaway, and S. Baig, 1978: Geostationary satellite observations of Gulf Stream meanders: Infrared measurements and time series analysis. *J. Geophys. Res.,* **83** (C12), 6123–6135.

Plaut, G., and R. Vautard, 1994: Spells of low-frequency oscillations and weather regimes in the Northern Hemisphere. *J. Atmos. Sci.,* **51,** 210–236.

Preisendorfer, R. W., 1988: *Principal Component Analysis in Meteorology and Oceanography.* Elsevier, 425 pp.

Qiu, B., 1994: Determining the mean Gulf Stream and its recirculations through combining hydrographic and altimetric data. *J. Geophys. Res.,* **99,** 951–962.

Reynolds, R. W., and T. M. Smith, 1994: Improved global sea surface temperature analysis using optimum interpolation. *J. Climate,* **7,** 929–948.

Richardson, P., 1985: Average velocity and transport of the Gulf Stream near 55°W. *J. Mar. Res.,* **43,** 83–111.

Semtner, A. J. J., and R. Chervin, 1992: Ocean general circulation from a global eddy-resolving model. *J. Geophys. Res.,* **97,** 5493–5550.

Speich, S., H. Dijkstra, and M. Ghil, 1995: Successive bifurcations in a shallow-water model applied to the wind-driven ocean circulation. *Nonl. Proc. Geophys.,* **2,** 241–268.

Stammer, D., R. Tokmakian, A. Semtner, and C. Wunsch, 1996: How well does a 1/4° global circulation model simulate large-scale oceanic observations? *J. Geophys. Res.,* **101,** 25 779–25 811.

Trenberth, K., J. Olson, and W. Large, 1989: A global ocean wind stress climatology based on ECMWF analyses. NCAR Tech. Note TN-338+Str, 93 pp. [Available from National Center for Atmospheric Research, 1850 Table Mesa Dr., Boulder, CO 80307.]

Vautard, R., and M. Ghil, 1989: Singular spectrum analysis in nonlinear dynamics with applications to paleoclimatic time series. *Physica D,* **35,** 395–424.

——, P. Yiou, and M. Ghil, 1992: Singular spectrum analysis: A toolkit for short, noisy chaotic signals. *Physica D,* **58,** 95–126.

Vazquez, J., 1993: Observations on the long-period variability of the Gulf Stream downstream of Cape Hatteras. *J. Geophys. Res.,* **98** (C11), 20 133–20 147.

——, V. Zlotnicki, and L.-L. Fu, 1990: Sea level variabilities in the Gulf Stream between Cape Hatteras and 50° W: A Geosat study. *J. Geophys. Res.,* **95** (C10), 17 957–17 964.

von Storch, H., G. Buerger, R. Schnur, and J.-S. von Storch, 1995: Principal oscillation patterns: A review. *J. Climate,* **8,** 377–400.

Vossepoel, F., 1995: Processing of altimeter and infrared radiometer data for eddy detection in the Gulf Stream. M.S. thesis, Faculty of Aerospace Engineering, Delft University of Technology, Delft, Netherlands, 133 + viii pp.

Wang, L., and C. Koblinsky, 1995: Low-frequency variability in regions of the Kuroshio Extension and the Gulf Stream. *J. Geophys. Res.,* **100** (C9), 18 313–18 331.

——, and ——, 1996: Annual variability of the subtropical recirculations in the North Atlantic and North Pacific: A TOPEX/Poseidon study. *J. Phys. Oceanogr.,* **26,** 2462–2479.

——, ——, and S. Howden, 1998: Annual and intra-annual sea level variability in the region of the Kuroshio Extension from TOPEX/Poseidon and Geosat altimetry. *J. Phys. Oceanogr.,* **28,** 692–711.

Weare, B. C., and J. N. Nasstrom, 1982: Examples of extended empirical orthogonal function analyses. *Mon. Wea. Rev.,* **110,** 481–485.